Inorganic Chemistry

Article

pubs.acs.org/IC

From a Dy(III) Single Molecule Magnet (SMM) to a Ferromagnetic [Mn(II)Dy(III)Mn(II)] Trinuclear Complex

Asamanjoy Bhunia,[†] Michael T. Gamer,[†] Liviu Ungur,[‡,§] Liviu F. Chibotaru,*[,‡] Annie K. Powell,*[,†,∥] Yanhua Lan,*[,†] Peter W. Roesky,*[,†] Fabian Menges,[⊥] Christoph Riehn,[⊥] and Gereon Niedner-Schatteburg[⊥]

[†]Institut für Anorganische Chemie, Karlsruher Institut für Technologie (KIT), Engesserstr. 15, 76128 Karlsruhe, Germany

[‡]Division of Quantum and Physical Chemistry, Katholieke Universiteit Leuven, Celestijenlaan 200F, 3001 Leuven, Belgium

[§]INPAC—Institute of Nanoscale Physics and Chemistry, Katholieke Universiteit Leuven, Celestijenlaan 200F, 3001 Leuven, Belgium

[∥]Institut für Nanotechnologie, Karlsruher Institut für Technologie (KIT), Postfach 3640, D-76021 Karlsruhe, Germany

[⊥]Fachbereich Chemie, Technische Universität Kaiserslautern und Landesforschungszentrum OPTIMAS, Erwin-Schrödinger-Straße, Gebäude 52, 67663 Kaiserslautern, Germany

Supporting Information

ABSTRACT: The Schiff base compound 2,2′-{[(2-aminoethyl)imino]bis[2,1-ethanediyl-nitriloethylidyne]}bis-2-hydroxy-benzoic acid (H_4L) as a proligand was prepared *in situ*. This proligand has three potential coordination pockets which make it possible to accommodate from one to three metal ions allowing for the possible formation of mono-, di-, and trinuclear complexes. Reaction of *in situ* prepared H_4L with $Dy(NO_3)_3{\cdot}5H_2O$ resulted in the formation of a mononuclear complex $[Dy(H_3L)_2](NO_3){\cdot}(EtOH){\cdot}8(H_2O)$ (**1**), which shows SMM behavior. In contrast, reaction of *in situ* prepared H_4L with $Mn(ClO_4)_2{\cdot}6H_2O$ and $Dy(NO_3)_3{\cdot}5H_2O$ in the presence of a base resulted in a trinuclear mixed 3d−4f complex $(NHEt_3)_2[Dy\{Mn(L)\}_2](ClO_4){\cdot}2(H_2O)$ (**2**). At low temperatures, compound **2** is a weak ferromagnet. Thus, the SMM behavior of compound **1** can be switched off by incorporating two Mn(II) ions in close proximity either side of the Dy(III). This quenching behavior is ascribed to the presence of the weak ferromagnetic interactions between the Mn(II) and Dy(III) ions, which at $T > 2$ K act as a fluctuating field causing the reversal of magnetization on the dysprosium ion. Mass spectrometric ion signals related to compounds **1** and **2** were both detected in positive and negative ion modes via electrospray ionization mass spectrometry. Hydrogen/deuterium exchange (HDX) reactions with ND_3 were performed in a FT-ICR Penning-trap mass spectrometer.

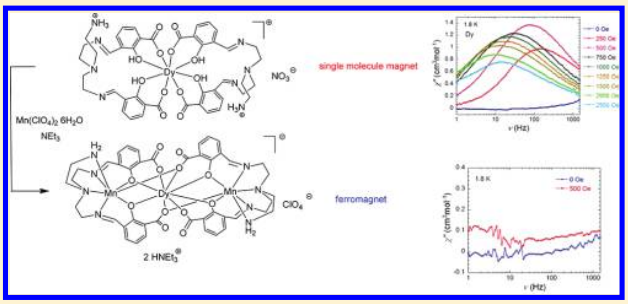

INTRODUCTION

The discovery of the first single molecule magnet (SMM) in the beginning of the 1990s stimulated a huge number of research groups to pursue SMMs due to their potential use in information storage.[1−3] A large number of polynuclear transition metal complexes with various topologies and behaving as SMMs has been reported. In recent years, lanthanide-containing SMMs have attracted great interest because of the large single-ion magnetic anisotropies stabilized by many configurations and especially the Dy(III) ion.[4−15] Out of these, only a few cases containing a single paramagnetic lanthanide ion giving rise to SMM behavior have been reported.[16−26] Among the early results reported are the phthalocyanine (Pc) double-decker complexes $[Pc_2Ln]$ (Ln = Tb(III) and Dy(III)) of Ishikawa et al.[16,24] They exhibit very large energy barriers for the relaxation of magnetization. Coronado and co-workers also have reported similar slow relaxation for a single lanthanide(III) ion sandwiched between two polyoxometalate ligands.[18,22,23]

In addition to pure 3d and pure 4f SMMs, much attention in this field is currently being paid to the synthesis and investigation of heterometallic SMMs featuring both 3d and 4f metal ions. The motivation of this approach is to achieve high spin ground states (S) via the involvement of 3d metal ions in conjunction with the large single-ion anisotropy (D) associated with 4f ions. Although the rare-earth ions efficiently introduce anisotropy, the coupling between 4f−4f ions is usually very weak compared to that of 3d−3d ions and represents a potentially major drawback to enhancing SMM behavior.[27] Many recent results have demonstrated that the observation of SMM behavior is no longer adequately described using simple D and S parameters; careful consideration of the overall symmetry of the complex in particular with the orientation of the anisotropy axes in terms of the lanthanide ions should be made.[28,29]

Received: January 11, 2012
Published: April 20, 2012

   dx.doi.org/10.1021/ic300065x | *Inorg. Chem.* 2012, 51, 9589−9597

Herein, we report on the synthesis of a mononuclear Dy(III) complex which exhibits SMM behavior. Furthermore, we show that the SMM behavior can be switched off by incorporating two Mn(II) ions in the pockets on either side of the Dy(III) ion. The added Mn−Dy exchange coupling, being significantly lower than the temperatures at which magnetic blocking was investigated, acts on the dysprosium ion as a fluctuating magnetic field which causes the reversal of Dy magnetization, much as the intermolecular magnetic interaction does in SMMs. This work indeed suggests that the combination of both 3d and 4f ions into one system may not always be an advantage: the enhancement of SMM behavior in such complexes necessarily requires strong exchange interaction between the metal sites.

EXPERIMENTAL SECTION

General Considerations. Elemental analyses were carried out with an Elementar vario EL analyzer. IR spectra were obtained on a Bruker IFS 113v FTIR spectrometer. ICP-AES measurements were performed using a Varian Liberty 150 spectrometer. 3-Formyl salicylic acid, tris-(2-aminoethyl)amine, $Dy(NO_3)_3{\cdot}5H_2O$, $Mn(ClO_4)_2{\cdot}6H_2O$, $Y(NO_3)_3{\cdot}6H_2O$, and all solvents were used as purchased from commercial sources without further purification.

Magnetic Measurements. The magnetic measurements were carried out with the use of a Quantum Design SQUID magnetometer MPMS. This magnetometer works between 1.8 and 400 K for dc applied fields ranging from −70 to +70 kOe. Measurements were performed on the polycrystalline samples dispersed in Apeizon grease. The magnetic data were corrected for the sample holder and the diamagnetic contribution estimated from Pascal constants.

*$[Dy(H_3L)_2](NO_3){\cdot}(EtOH){\cdot}8(H_2O)$ (**1**).* To a stirred solution of 3-formylsalicylic acid (68 mg, 0.41 mmol) in ethanol/water (15 mL/5 mL) was added tris-(2-aminoethyl)amine (0.03 mL, 0.2 mmol), followed by the addition of $Dy(NO_3)_3{\cdot}5H_2O$ (47 mg, 0.11 mmol). The resulting solution was then stirred for 12 h at room temperature, filtered, and left undisturbed. After 2 days, yellow block-shaped crystals were collected, washed with cold ethanol, and dried in a vacuum. Yield: 53 mg of single crystals (38% based on Dy). Anal. Calcd. for $C_{44}H_{58}DyN_9O_{19}$ (corresponds to **1** − 4(H_2O) − EtOH): C, 44.80; H, 4.96; N, 10.69 Found: C, 44.99; H, 5.02; N, 10.61. IR (KBr): ν 3420 (br), 3049 (br), 2951 (w), 2825 (w), 1650 (s), 1609 (s), 1538 (s), 1452 (m), 1381 (s), 1221 (m), 1187 (m), 1145 (m), 1031 (m), 867 (m), 762 (m), 641 (m), 628 (w), 445 (w) cm^{-1}.

*$(NHEt_3)_2[Dy\{Mn(L)\}_2](ClO_4){\cdot}2(H_2O)$ (**2**).* 3-Formyl salicylic acid (67 mg, 0.4 mmol) and tris-(2-aminoethyl)amine (0.03 mL, 0.2 mmol) were dissolved in an ethanol/water (15 mL/5 mL) mixture. Then, triethylamine (0.14 mL, 1 mmol) was added dropwise with stirring. To the resulting solution were added $Mn(ClO_4)_2{\cdot}6H_2O$ (75 mg, 0.21 mmol) and $Dy(NO_3)_3{\cdot}5H_2O$ (47 mg, 0.11 mmol), and the subsequent mixture was stirred for another 12 h. The solution was then filtered and left undisturbed. Within a few days, yellow crystals had formed and were collected, washed with diethyl ether, and dried in a vacuum. Yield: 48 mg of single crystals (30% based on Dy). Anal. Calcd. for $C_{56}H_{80}ClDyMn_2N_{10}O_{18}$: C, 45.17; H, 5.41; N, 9.41. Found: C, 44.71; H, 5.34; N, 9.26. IR (KBr): ν 3451 (w), 3480 (w) 3415 (w), 3283 (w), 3232 (w), 2906 (w), 2857 (w), 1637 (s), 1594 (m), 1553 (s), 1440 (m), 1416 (s), 1405 (w), 1332 (w), 1298 (m), 1227 (m), 1194 (w), 1159 (m), 1093 (s), 1026 (m), 962 (m), 878 (s), 832 (m), 802 (m), 764 (s), 666 (w), 623 (s), 476 (w) cm^{-1}.

Alternative Route. Compound **1** $[Dy(H_3L)_2](NO_3){\cdot}(EtOH){\cdot}8(H_2O)$ (32 mg, 0.02 mmol) and triethylamine (0.02 mL, 0.14 mmol) were dissolved in $EtOH/H_2O$ (10 mL/2 mL), and the resulting yellow solution was stirred for 5 min, after which $Mn(ClO_4)_2{\cdot}6H_2O$ (75 mg, 0.21 mmol) was added and the subsequent mixture stirred for 5 h. The solution was then filtered and left undisturbed. After 3 days, yellow crystals were collected, washed with diethyl ether, and dried in a vacuum. Yield: 11 mg of single crystals (30%, based on compound **1**). The lattice constants were measured to determine the identity.

$[Y_{0.805}Dy_{0.195}(H_3L)_2](NO_3){\cdot}(EtOH){\cdot}8(H_2O)$. The dysprosium complex was diluted into the diamagnetic yttrium host with a Dy/Y ratio of 20:80. The synthetic procedure described above for compound **1** was repeated starting from 133 mg (0.8 mmol) of 3-formyl salicylic acid, 0.06 mL (0.4 mmol) of tris-(2-aminoethyl)amine, 18.1 mg (0.04 mmol) of $Dy(NO_3)_3{\cdot}5H_2O$, and 58.9 mg (0.16 mmol) of $Y(NO_3)_3{\cdot}6H_2O$. The crystals obtained were analyzed by ICP-AES, and the composition was found to be Dy = 2.78% and Y = 6.28% in weight. This results in the molecular formula $[Y_{0.805}Dy_{0.195}(H_3L)_2](NO_3){\cdot}(EtOH){\cdot}8(H_2O)$.

Details of the X-Ray Diffraction Measurement, Structure Solution, and Refinement. *General.* Data were collected on a diffractometer equipped with a STOE imaging plate detector system IPDS2 using Mo Kα radiation with graphite monochromatization (λ = 0.71073 Å) at 200 K. Structure solution was performed by direct methods and full-matrix-least-squares refinement against F^2 using SHELXS-97 and SHELXL-97 software.[30]

*Crystal Data for **1**.* $C_{44}H_{50}DyN_8O_{12}{\cdot}(NO_3){\cdot}(EtOH){\cdot}8(H_2O)$, M = 1297.63 g/mol, triclinic, a = 12.9580(3) Å, b = 15.2000(4) Å, c = 16.4680(4) Å, α = 74.850(2)°, β = 66.944(2)°, γ = 71.621(2)°, V = 2796.72(12) Å^3, T = 173(2) K, space group $P\bar{1}$, Z = 2, μ(Mo Kα) = 1.425 mm^{-1}, 30 623 reflections measured, 12 726 independent reflections (R_{int} = 0.0979). The final R_1 values were 0.0429 ($I > 2\sigma(I)$). The final $wR(F^2)$ values were 0.1185 ($I > 2\sigma(I)$). The final R_1 values were 0.0449 (all data). The final $wR(F^2)$ values were 0.1199 (all data). The goodness of fit on F^2 was 1.063.

*Crystal Data for **2**.* $C_{44}H_{44}DyMn_2N_8O_{12}{\cdot}2(C_6H_{16}N){\cdot}(ClO_4){\cdot}2(H_2O)$, M = 1489.13 g/mol, triclinic, a = 10.8248(3) Å, b = 15.9097(5) Å, c = 19.8563(6) Å, α = 77.331(3)°, β = 85.548(3)°, γ = 73.002(2)°, V = 3190.30(16) Å^3, T = 200(2) K, space group $P\bar{1}$, Z = 2, μ(MoKα) = 1.667 mm^{-1}, 49 900 reflections measured, 7909 independent reflections (R_{int} = 0.0737). The final R_1 values were 0.0384 ($I > 2\sigma(I)$). The final $wR(F^2)$ values were 0.0937 ($I > 2\sigma(I)$). The final R_1 values were 0.0518 (all data). The final $wR(F^2)$ values were 0.1013 (all data). The goodness of fit on F^2 was 1.058.

Crystallographic data (excluding structure factors) for the structures reported in this paper have been deposited with the Cambridge Crystallographic Data Centre as supplementary publication nos. CCDC 820675 and 820676. Copies of the data can be obtained free of charge on application to CCDC, 12 Union Road, Cambridge CB21EZ, U.K. (fax: +(44)1223-336-033; e-mail: deposit@ccdc.cam.ac.uk).

Electrospray Ionization Mass Spectrometry (ESI MS). Electrospray ionization mass spectrometry (ESI MS) was performed on a Bruker Esquire 3000plus ion trap instrument in positive and negative ionization modes. The scan speed was 13 000 m/z/s in standard resolution scan mode (0.3 fwhm/m/z); the scan range was 15 to 2800 m/z. All spectra were accumulated for at least 2 min. Sample solutions in acetonitrile at concentrations of 1×10^{-4} M were used without further purification and continuously infused into the ESI chamber at a flow rate of 2 μL/min using a syringe pump. Nitrogen was used as a drying gas at a flow rate of 3.0 L/min at 300 °C. The solutions were sprayed at a nebulizer pressure of 4 psi, and the electrospray needle was typically held at 4.5 kV. The instrument was controlled by Bruker Esquire Control 5.3 software, and data analysis was performed using Bruker Data Analysis 3.4 software.

H/D exchange with ND_3 was performed under single collision conditions at a background pressure of approximately 1.0×10^{-8} mbar (Bruker Apex III FT-ICR-MS equipped with a 7.0-T magnet and an APOLLO I electrospray ion source). Sample solutions in acetonitrile at concentrations of about 1×10^{-4} M were continuously infused into the ESI chamber at a flow rate of 2 μL/min using a syringe pump. Nitrogen was used as a drying gas with a flow rate of 10.0 L/min at approximately 300 °C. The solutions were sprayed at a nebulizer pressure of 25 psi, and the electrospray needle was typically held at 4.0 kV. Transfer parameters to the Penning trap of the mass spectrometer were held constant.

dx.doi.org/10.1021/ic300065x | Inorg. Chem. 2012, 51, 9589−9597

Scheme 1. Synthesis of Compounds 1 and 2 (Simplified Drawing)

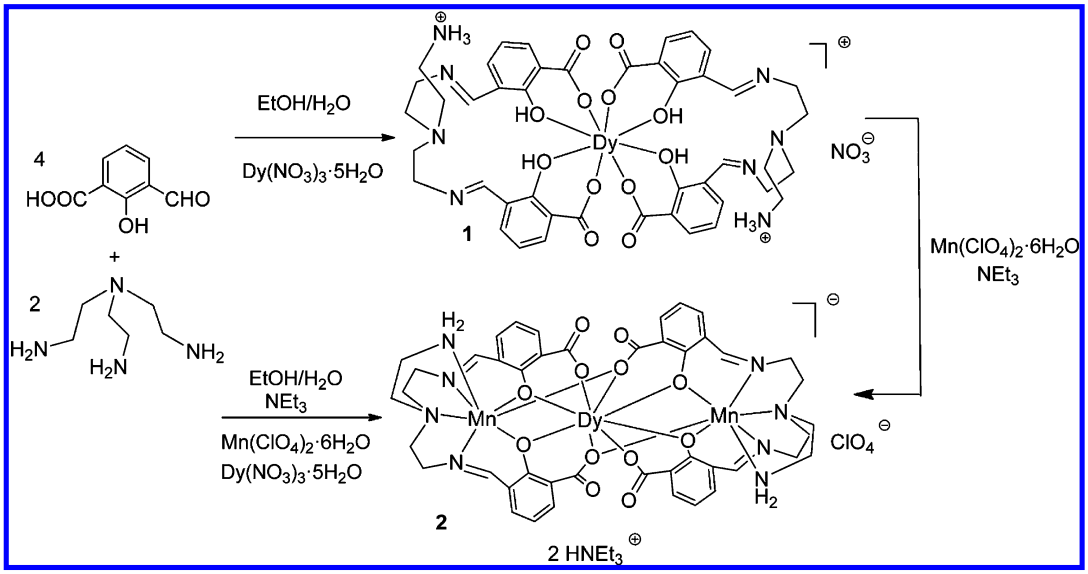

Theoretical Methods. *Ab initio* calculations of **1** and of Dy and Mn fragments in **2** were performed in the frame of a complete active space self-consistent field (CASSCF) approach using the MOLCAS package.[31] In the case of **1**, the entire complex was taken in the calculation. Due to the fact that the positions of four hydrogen atoms (H) bound to the four phenoxy oxygens (Scheme 1) could not be identified from the X-ray analysis of **1**, they were optimized at the Molecular Mechanics (MM) level using the program Avogadro.[32] The position of all other atoms was kept unchanged. The Dy fragment for complex **2** was built by substituting the magnetic Mn^{2+} ions by diamagnetic Zn^{2+} in the *ab initio* calculations. The Mn1 and Mn2 fragments from **2** were built by substituting the other magnetic Mn^{2+} ion by the diamagnetic Zn^{2+} and the magnetic Dy^{3+} ion by the diamagnetic La^{3+} ion. The position of all other atoms was kept intact (i.e., were taken from the X-ray structure) for all three mononuclear fragments. Two basis sets were used for **1**, 1-A and 1-B, and one single basis set for **2** (see the Supporting Information for computational details). The active space in the CASSCF calculations of **1** and of the Dy fragment from **2** included nine electrons in seven orbitals (i.e., the 4f shell of the Dy^{3+} ion). The active space in the CASSCF calculations of Mn fragments from **2** included five electrons in five orbitals (i.e., the 3d shell of the Mn^{2+} ion).

The relativistic effects were taken into account within the Douglas–Kroll–Hess Hamiltonian[33,34] combined with an efficient treatment of spin–orbit coupling via the atomic mean-field integral (AMFI) method,[35] both implemented in MOLCAS.[31] The scalar-relativistic terms of this Hamiltonian were included at the stage of the calculations of multiconfigurational CASSCF wave functions corresponding to definite total spin of the complex/fragment. In a second stage, the spin–orbit coupling terms were included within the restricted active space state interaction (RASSI-SO[35]) method, which uses the CASSCF wave functions as input states. This was done by mixing the calculated CASSCF wave functions corresponding to several low-lying spin terms within the module RASSI of MOLCAS package.[31] In the case of **1** and Dy fragment of **2**, this mixing involved 21 spin sextets, 128 spin quartets, and 130 spin doublets. In the case of Mn fragments from **2**, the spin–orbit mixing involved one spin sextet, 24 spin quartets, and 75 spin doublets arising from the d^5 electronic configuration of the Mn^{2+} ion. The resulting spin–orbit eigenstates, which are Kramers doublets for Dy and both Mn centers, were used for the calculation of the local *g* tensors, including the main magnetic (anisotropy) axis, for both complexes and of static magnetic properties (magnetic susceptibility and field-dependent magnetization) for **1**, using the SINGLE_ANISO module[36,37] recently implemented in MOLCAS-7.6.

The exchange spectrum in **2** was simulated using the Lines model,[38] as discussed in previous work,[36,37] with the software POLY-ANISO.[39] In the Lines model, the exchange matrix is simulated by matrix elements of an effective isotropic exchange Hamiltonian (H_{Lines}) written in the basis of low-lying spin–orbit multiplets on magnetic sites. In the present case, the minimal model includes two Lines parameters, J_1 and J_2, describing the Dy–Mn and Mn–Mn exchange interactions:

$$H_{Lines} = -J_1(\vec{S}\cdot\vec{S}_1 + \vec{S}\cdot\vec{S}_2) - J_2\vec{S}_1\cdot\vec{S}_2 \quad (1)$$

where S_1 and S_2 are the spins 5/2 on Mn^{II} ions and S is the spin 5/2 on the Dy^{III} ion. The lowest multiplets on the metal ions, on which the exchange Hamiltonian in eq 1 is projected, are the three Kramers doublets arising from the ground spin sextet of each Mn site and the eight Kramers doublets arising from the ground $J = 15/2$ on the Dy site.

RESULTS AND DISCUSSION

Synthesis and Structures. On the basis of 3-formylsalicylic acid, we prepared the hitherto unknown cage compound 2,2′-{[(2-aminoethyl)imino]bis[2,1-ethanediylnitriloethylidyne]}bis-2-hydroxy-benzoic acid, H_4L, *in situ* as a proligand. This ligand has three potential coordination pockets which make it possible to accommodate different numbers of metal ions, in the work reported here, leading to the formation of monomeric and trimeric complexes. The reaction of 3-formylsalicylic acid with tris-(2-aminoethyl)amine (2:1) in a mixture of ethanol/H_2O (3:1) followed by the addition of $Dy(NO_3)_3\cdot 5H_2O$ resulted in the formation of yellow crystals of the mononuclear complex $[Dy(H_3L)_2](NO_3)\cdot(EtOH)\cdot 8(H_2O)$ (**1**; Scheme 1). Compound **1** was characterized by standard analytical/spectroscopic techniques, and the solid state structure was determined by single-crystal X-ray diffraction (Figure 1a).

Compound **1** crystallizes in the triclinic space group $P\bar{1}$. The asymmetric unit found in the single crystal X-ray structure analysis of compound **1** contains a $[Dy(H_3L)_2]^+$ coordination cation (Figure 1a), a NO_3^- anion, one ethanol, and eight water molecules. In order to balance the charge, each ligand is singly negatively charged. Thus, the two acid groups are deprotonated, forming carboxylate functions, while the tethered amine

dx.doi.org/10.1021/ic300065x | Inorg. Chem. 2012, 51, 9589–9597

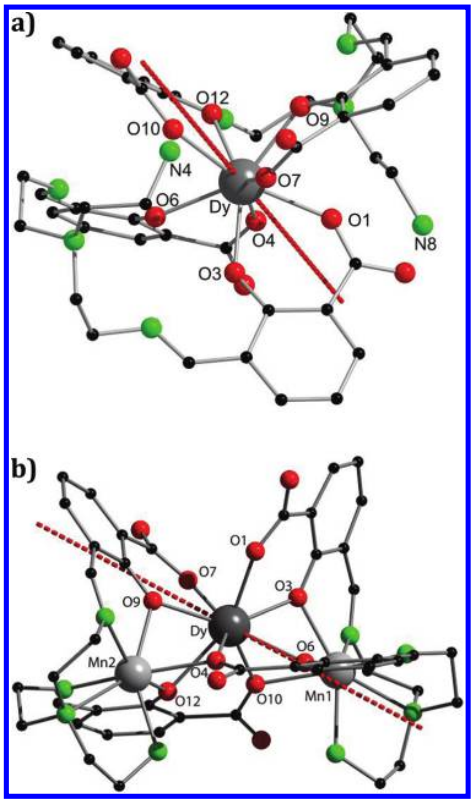

Figure 1. (a) Solid state structure of the $[Dy(H_3L)_2]^+$ cation of compound **1**. (b) Solid state structure of the $[Dy\{Mn(L)\}_2]^-$ anion of compound **2**, omitting hydrogen atoms for clarity. The color codes of balls: Dy, dark gray; Mn, light gray; O, red; N, green; C, black. The red dotted lines represent main anisotropy axes on the Dy ions in **1** (a) and **2** (b). Selected distances [Å] for **1**: Dy–O1 = 2.346(2), Dy–O3 = 2.325(2), Dy–O4 = 2.358(2), Dy–O6 = 2.374(2), Dy–O7 = 2.324(2), Dy–O9 = 2.324(2), Dy–O10 = 2.386(2), Dy–O12 = 2.358(2). Selected distances [Å] for **2**: Dy–O1 = 2.321(4), Dy–O3 = 2.335(3), Dy–O4 = 2.311(3), Dy–O6 = 2.381(4), Dy–O7 = 2.311(4), Dy–O9 = 2.329(3), Dy–O10 = 2.339(4), Dy–O12 = 2.430(4), Mn1–O3 = 2.231(4), Mn1–O6 = 2.293(4), Mn1–O10 = 2.247(4), Mn1–N1 = 2.256(5), Mn1–N2 = 2.621(1), Mn1–N3 = 2.208(5), Mn1–N4 = 2.277(5), Mn2–O4 = 2.262(4), Mn2–O9 = 2.246(4), Mn2–O12 = 2.285(4), Mn2–N5 = 2.245(5), Mn2–N6 = 2.652(1), Mn2–N7 = 2.2221(5), Mn2–N8 = 2.261(5), Dy–Mn1 = 3.4039(9), Dy–Mn2 = 3.4082(8).

is protonated, giving an NH_3^+ function. The $[Dy(H_3L)_2]^+$ cation contains one Dy(III) ion coordinated by two such ligands. Thus, the metal atom is coordinated by four phenolic oxygen atoms and four carboxyl oxygen atoms from both ligands, resulting in an 8-fold coordinated geometry. The coordination polyhedron can be best described as a distorted square antiprism. The Dy–O(phenoxy) and Dy–O(carboxyl) distances for the mononuclear compound are in the ranges 2.324(2)–2.374(2) Å and 2.324(2)–2.386(2) Å, respectively. Formally, each phenolic oxygen is protonated, but we could not locate the protons in the difference Fourier map. Moreover, there is no significant difference in the Dy–O bond lengths of the phenolic and the carboxyl groups. The shortest Dy–Dy′ distance is 9.313 Å. A plot showing the packing of the ions is shown in Figure S23, which shows that the counteranions and solvent molecules are embedded between the relatively large $[Dy(H_3L)_2]^+$ cations. The structure of the cation is supported by ESI MS data (see below).

Reaction of *in situ* prepared $\mathbf{H_4L}$ in an EtOH/H_2O (3:1) mixture with triethylamine, $Mn(ClO_4)_2{\cdot}6H_2O$, and $Dy(NO_3)_3{\cdot}5H_2O$ (10:2:1) resulted in the trinuclear mixed 3d–4f complex $(NHEt_3)_2[Dy\{Mn(L)\}_2](ClO_4){\cdot}2(H_2O)$ (**2**) (Scheme 1). The slight excess of triethylamine is essential for the formation of the mixed 3d–4f metal complex. The basic reaction conditions promote the complete deprotonation of the ligand, thus enabling the coordination to the manganese(II) ions. Compound **2**, which can also be obtained by a reaction of compound **1** with $Mn(ClO_4)_2{\cdot}6H_2O$ in the presence of a base, was characterized by standard analytical/spectroscopic techniques, and the solid state structure was determined by single crystal X-ray diffraction (Figure 1b). Compound **2** crystallizes in the triclinic space group $P\bar{1}$. The asymmetric unit contains two $(NHEt_3)^+$ cations, one $(ClO_4)^-$, one $[Dy\{Mn(L)\}_2]^-$ coordination anion, and two water molecules. The trimetallic $[Dy\{Mn(L)\}_2]^-$ anion is built up of a central Dy(III) atom, as observed in compound **1**, and two adjacent Mn(II) ions, which are coordinated in the outer pockets of both ligands (Figure 1b). In contrast to compound **1**, the two ligands are now fully deprotonated and, thus, have additional coordination sites available. The coordination mode of the Dy(III) atom is quite similar to the one observed in compound **1**. Again, the Dy(III) atom is 8-fold coordinated, being in the center of a distorted square antiprism coordination polyhedron. Although the ligand is now fully deprotonated, there is no significant difference in the Dy–O distances (2.311(4)–2.430(4) Å) in comparison to compound **1**. The two Mn(II) ions are 7-fold coordinated by four nitrogen atoms of the tris-(2-aminoethyl)amine subunit and three oxygen atoms of which two are phenoxy groups and the remaining one is part of a carboxyl group. The coordination polyhedron is best described as a distorted capped octahedron. As expected, the Mn–N bond distances of the amine nitrogen atoms (Mn1–N2 = 2.621(1) Å and Mn2–N6 = 2.652(1) Å) are significantly longer than those of the imine nitrogen atoms (2.208(5)–2.277(5) Å). The Dy–Mn distances of Dy–Mn1 = 3.4039(9) Å and Dy–Mn2 = 3.4081(8) Å show the close proximity of the metal atoms.

Electrospray Ionization Mass Spectrometry. Mass spectrometric ion signals related to compounds **1** and **2** were both detected in positive and negative ion modes via ESI MS. In the negative ion mode, we observed $[Dy(H_2L)_2]^-$ (doubly deprotonated cation of compound **1**, $Dy(C_{22}H_{24}N_4O_6)_2$) at 1044.38 *m*/*z* most abundant mass and $[Dy\{Mn(L)\}_2]^-$ (anion of compound **2**, $Dy(MnC_{22}H_{22}N_4O_6)_2$) at 1150.29 *m*/*z* most abundant mass. In the positive ion mode, we observed $[Dy(H_3L)_2]^+$ (cation of compound **1**) at 1046.29 *m*/*z* most abundant mass and $[Dy\{Mn(HL)\}_2]^+$ (doubly protonated anion of compound **2**) at 1152.15 *m*/*z* most abundant mass. All assignments were confirmed by simulations of the corresponding characteristic isotope patterns (Figures MS-S1a,b, MS-S2a,b), clearly supporting the X-ray analysis. The mass spectra recorded in the positive ion mode exclusively show peaks assigned to $[Dy(H_3L)_2]^+$ and $[Dy\{Mn(HL)\}_2]^+$, respectively, whereas in the negative ion mode, several fragments and adducts of the compounds **1** and **2** were detected (Figures MS-S3, MS-S4). From additional MS^n experiments on the species $[Dy\{Mn(HL)\}_2]^+$, a partially parallel and partially sequential loss of up to two CO_2 and two H_2O molecules was found with retention of the trinuclear metal core (see fragmentation scheme MS-S5, Figure MS-S6). MS^n experiments on [Dy-

dx.doi.org/10.1021/ic300065x | *Inorg. Chem.* 2012, 51, 9589–9597

$(H_3L)_2]^+$ gave a similar stepwise loss of CO_2 and H_2O (Figure MS-S7). In order to further elucidate the gas phase structure of $[Dy(H_3L)_2]^+$ and $[Dy\{Mn(HL)\}_2]^+$, hydrogen/deuterium exchange (HDX) reactions with ND_3 were performed in a FT-ICR Penning-trap mass spectrometer. As a result, a consecutive exchange of up to 10 hydrogen atoms in the case of $[Dy(H_3L)_2]^+$ was obtained. $[Dy\{Mn(HL)\}_2]^+$ showed only an exchange of two hydrogen atoms, even after a storage time of 960 s, although there are four more hydrogen atoms available on the amine groups (Figures MS-S8, MS-S9). We believe that this result indicates strong coordination of the amine groups to the manganese ions. The HDX results together with the fragmentation behavior (loss of H_2O) imply that probably the two exchangeable protons are not coordinated at the amine groups but at the carboxyl binding sites.

Magnetism. At room temperature, the χT products for **1** and **2** under an applied DC field of 1000 Oe are consistent with the expected values for one isolated Dy(III) ion ($S = {}^5/_2$, $L = 5$, $g = {}^4/_3$, $C = 14.17$ cm^3 K mol^{-1}) and one Dy(III) ion and two Mn(II) ($S = {}^5/_2$, $g = 2$, $C = 4.375$ cm^3 K mol^{-1}) ions, respectively. The χT product of **1** decreases monotonically over the whole temperature range down to 2 K, but that of **2** first steadily decreases to approach a minimum of 20.95 cm^3 K mol^{-1} at 10 K and then increases to reach 23.41 cm^3 K mol^{-1} at 1.8 K (Figure 2). For both, the decrease in the χT value with

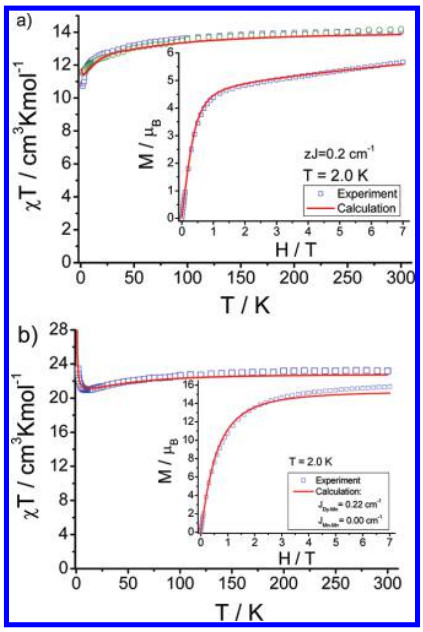

Figure 2. Measured (empty squares and circles) and calculated (line) temperature dependence of χT for **1** (a) and **2** (b) for the first set of exchange parameters ($J_{Dy-Mn} = 0.22$ cm^{-1}; $J_{Mn-Mn} = 0.0$ cm^{-1}, see Supporting Information). Inset: molar magnetization at 2 K. In (a), circles show the χT for the diluted Dy−Y complex, while the squares correspond to the pure (undiluted) compound **1**. The values of exchange parameters correspond to $S = 1/2$ on Dy(III) and $S = 5/2$ on Mn(II).

temperature is principally the result of thermal depopulation of the Stark sublevels of the Dy(III) ion, but in the case of **2**, the increase of χT below 10 K also indicates weak ferromagnetic interactions between the Mn(II) and Dy(III) ions. In line with this, the field dependence of the magnetization at 2 K shows that the magnetization of **1** does not saturate but reaches 5.6 μB with a linear slope observed at high field (>20 kOe), indicating anisotropy in the system (Figure 2a and S1), whereas the magnetization of compound **2** increases relatively fast at low fields and almost approaches a saturation of 15.8 μB (Figure 2b and S7) at 70 kOe. The magnetization value of 15.8 μB is in approximate agreement with that expected of 15.0 μB, this being the sum of that for one Dy(III) (5.0 μB, for axial and rigid moment) and two Mn(II) (5.0 μB, for weak exchange coupling) ions.

Ab Initio Calculations. The calculated main values of the ground state g tensors and orientations of the main magnetic axes on the Dy ion in **1** and **2** are given in Table 1 and Figure 1,

Table 1. Main Values of the g Tensors of the Ground Kramers Doublet on Dy Ion in 1 and 2

	1	2
g_X	0.0238	0.0682
g_Y	0.0445	0.1542
g_Z	18.7688	19.3367

respectively. The main magnetic axis in **1** (defined as z) lies almost in the O4−O7−O10 plane (Figure 1a), close to the Dy−O4 bond (12°). In **2**, the main magnetic axis lies almost in the O4−O6−O7 plane (Figure 1b) and makes an angle of 81° with the Mn1−Mn2 axis. As mentioned above, the positions of the hydrogen atoms close to O3, O6, O9, and O12 in **1** (Figure 1a) are not available from structural data and have been obtained, therefore, from molecular mechanics optimization. In order to correct the errors introduced by this procedure, the first excited Kramers doublet was slightly shifted from the calculated value (see Supporting Information). Figure 2a shows the calculated susceptibility and magnetization for **1**. The exchange spectrum in **2** has been simulated by the Lines model, as discussed in the Theoretical Methods. The two Lines parameters describing the Dy−Mn and Mn1−Mn2 exchange interactions were derived from the fitting of χT(T) and M(T) data for **2** (Figure 2b). The exchange spectrum arising from the interaction of the ground Kramers doublet on Dy with $S = {}^5/_2$ on Mn1 and Mn2 ($2 \times 6 \times 6 = 72$ exchange states =36 exchange Kramers doublets) has a spread of only 1.13 cm^{-1} (see Table S6), which is the result of a very weak Dy−Mn exchange interaction. However, the zero-field splitting obtained for the Mn sites is even smaller, *ca.* 0.2 cm^{-1} (Table S3). This is the reason why the local magnetizations on Mn1 and Mn2 in exchange states are not directed along the corresponding anisotropy axes but are tilted toward the anisotropy axis on Dy (Figure S14). Due to the small exchange splitting, complex **2** is found in the "paramagnetic regime", where the magnetic ions are essentially uncoupled for all temperatures at which the measurements were done (Figure 2b). Further confirmation of this is given by the difference between experimental M(H) for **2** and **1**, which is already very close to the sum of magnetizations for Mn1 and Mn2 at $T = 2$ K (Figure S19). The small discrepancy is due to nonequivalence of the Dy ions in **1** and **2** (Table S2 and Figure 1).[40−42]

Magnetization Dynamics. The magnetization dynamics of both complexes was probed using AC measurements. In the absence of a static magnetic field, no appreciable out-of-phase component of the AC susceptibility could be observed in either complex (Figures S2, S3, and S8). However, for the mononuclear Dy^{III} complex **1**, the intensity of the out-of-phase component of the AC susceptibility becomes significantly

dx.doi.org/10.1021/ic300065x | Inorg. Chem. 2012, 51, 9589−9597

enhanced with the application of an external DC field (Figure S3), and field-dependence of the AC susceptibility measurements under a static field was studied in detail. These make it possible to suppress the QTM, thereby enabling the investigation of the characteristic parameters of the magnetic relaxation of a given SMM. For the undiluted compound, a 2000 Oe field was found to be optimum for slowing down the relaxation process. A similar behavior could be observed for the diluted sample by applying a field of 200 Oe (Figure S3, S4). Subsequent frequency sweeping AC susceptibility measurements were carried out using 200 and 2000 Oe fields for the diluted and pure sample, respectively (Figure S5). As shown in Figure 3, the relaxation time below 2.4 K almost reaches a

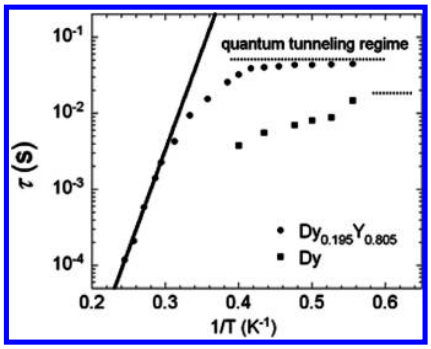

Figure 3. The relaxation time of **1** in a pure and diluted form as a function of temperature. The solid line represents a thermally activated Arrhenius law; parameters are discussed in the text. The dotted lines indicate the quantum tunneling regimes.

constant value of 0.04 s, indicating that the relaxation mechanism in this regime operates via quantum tunneling between the two degenerate Kramers ground states. On increasing the $1/T$ value, the observed relaxation time progressively increases exponentially. The magnetic relaxation which is attributed to the Orbach process is thermally activated between 3.4 and 4.1 K. This kind of quantum relaxation behavior has recently been documented for a few lanthanide-based SMM clusters in which the mechanism of the relaxation has been investigated using the techniques of magnetic dilution.[18,25,26,42,49]

In order to verify the intrinsic molecular nature of the magnetic behavior, measurements were performed on a sample of **1** diluted in a diamagnetic ($[Y(H_3L)_2]^+$) matrix with a molar ratio of 19.5:80.5 (see Supporting Information). The DC magnetic data above 10 K are almost identical with those of the pure compound except that the low-temperature χT product does not decrease as rapidly as that of the pure compound (Figure S1). Although at first glance this seems to indicate the presence of intermolecular AF interactions in **1**, the upturn of χT in Figure 2a at $T < 2$ K may indicate that these interactions are actually ferromagnetic (see the enlargement in Figure S9). Furthermore, the out-of-phase components of the AC susceptibilities are strongly frequency dependent and can be detected in the diluted sample even down to a frequency of 1 Hz (Figure S2).

The characteristic parameters of the relaxation process were then extracted by fitting the AC data with a thermally activated Arrhenius relaxation law, $\tau = \tau_0 \exp(U_{eff}/k_BT)$. Linear behavior was established between 3.4 and 4.1 K (solid line, Figure 3), giving an effective energy barrier of U_{eff} = 60.4 K and a relaxation time of $\tau_0 = 4.4 \times 10^{-11}$ s. These parameters are comparable with those recently reported for a mononuclear DyDOTA SMM.[49] It is important to note that for the undiluted sample the relaxation process could only be detected below 2.5 K in the measurement window of a magnetometer such as ours (Figure S5), which underlines the value of dilution experiments (well-known in other branches of electronic structure investigation) as well as the prospects for new instrumentation. As a check, the breadth of the distribution of the relaxation processes in a Cole−Cole plot of the in-phase versus out-of-phase susceptibilities was analyzed using a generalized Debye model. The obtained α value for compound **1** varies from 0.51 to 0.75 (Figure S6 and Table S1) and 0.51 to 0.56 (Figure S6 b and Table S1) in a pure and diluted form, respectively. An explanation for these large values of α and their weak dependence on the dilution is given below.

Effect of Intermolecular Interactions and Disorder. To understand the magnetic properties of pure and diluted compound **1**, it is first necessary to assess the strength of intermolecular interactions. Antiferromagnetic intermolecular interactions would lead to a decrease in χT at low temperatures, thus enhancing the decrease of susceptibility arising from the depopulation of crystal-field-split Stark levels on the Dy ion. On the other hand, ferromagnetic intermolecular interactions would always result in an increase in χT at some temperature, no matter how weak these interactions are. Figures 2a and S9 show that a small upturn of χT is indeed present in both pure and diluted samples of **1**. The simulation of the position of this upturn (T = 2 K) gives the value zJ = 0.1 cm^{-1} (with respect to S = 1/2 on Dy(III) centers). However, as Figure S9 shows, the shapes of experimental and simulated curves look completely different, and this leaves us with the conclusion that the sharp upturn seen here in the experimental curves for both pure and undiluted complex **1**, which can only be simulated at temperatures very close to zero and never at T = 2 K, is probably not simply a result intermolecular interactions.

Another way to assess the strength of intermolecular interactions is a direct calculation of dipolar interaction energy between the magnetic moment of a given Dy ion with the moments of surrounding complexes (the exchange interaction between complexes is negligible due to a large separation of ca. 10 Å between the Dy ions). The results of these calculations using the *ab initio* determined ground state g tensor (Table 1, Figure 1a) is given in Figure 4a for an undiluted sample **1** of spherical shape. We can see that this energy is positive, meaning that for large enough samples the dipolar term at $E_{dip} \approx 0.06$ cm^{-1} will be sufficient to impose an antiferromagnetic intermolecular interaction. This term corresponds to the parameter $zj = -E_{dip}/(1/2 \times 1/2) \approx -0.24$ cm^{-1}, for which the calculated χT at low temperatures shows a downturn compared with the undiluted sample (Figure S9). The obtained value of zJ is rather weak at 1 order of magnitude less than in some recently investigated dysprosium complexes,[50] for which $zJ = -1.84$ cm^{-1} was derived. Next, we estimated the dependence of E_{dip} on the shape of the sample. Figure 4b shows the dipolar interaction energy for a parallelepiped-like sample with the long side oriented along one of the crystallographic axes. We can see that for these shapes the interaction is also predominantly antiferromagnetic. Moreover, the order of magnitude of E_{dip} remains the same as in the case of spherical sample (Figure 4a).[51]

The estimated intermolecular interaction seems too weak to explain the observed differences in χT for diluted and undiluted compound **1**, which reach much higher temperatures than the

dx.doi.org/10.1021/ic300065x | Inorg. Chem. 2012, 51, 9589−9597

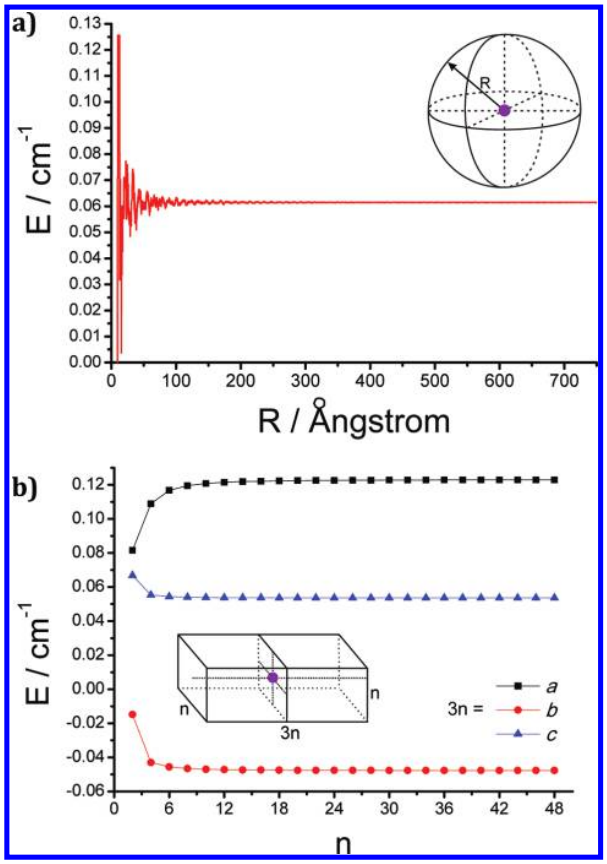

Figure 4. The energy of the intermolecular dipolar interaction of one Dy magnetic moment (violet circle) in an undiluted sample of **1** with neighbor Dy sites as a function of the size of the sample of spherical shape (a) and a parallelepiped like shape (b) with the long side 3*n* taken along one of the crystallographic axes (*n* is the number of unit cells taken along one of the short sides). The directions of anisotropy axes on Dy sites are taken from *ab initio* calculation **1-B** (see the text).

predicted values for this interaction (Figures 2a and S9). Most importantly, Figure S9 shows that the χT curve for the undiluted sample (for which the antiferromagnetic interaction is stronger) passes above the corresponding curve for the diluted sample at $T > 5$ K. For this, the observed differences in χT should be mainly attributed to differences in the electronic structure of individual complexes in these samples. This can result from differences in hydrogen-bonding interactions which can be significantly affected by changes in the Lewis acidity of the local metal-ion centers. In the case of compound **1**, for example, there are different possibilities for the hydrogens bonded to the four phenolic oxygens (Scheme 1) in diluted and undiluted samples of **1**, which in turn will have a strong effect (mediated by the oxygen ions) on the crystal field of the Dy^{III} ions. Such strong effects dictated by the positions of covalently bonded atoms from the second coordination sphere of a metal ion have been recently reported in terms of the influence on zero-field splitting of Co complexes.[53] Moreover, since some of the hydrogen atoms mentioned above could not be located in the single crystal X-ray structure analysis (see above), it is likely that they are positionally disordered even in the undiluted complex **1**. These two considerations point toward the fact that local hydrogen-bonding considerations are an important factor in determining the possibilities for relatively strong secondary dipolar effects within crystals containing SMMs. The role of supramolecular interactions between SMMs is by no means unprecedented. In addition to the bias which can result between hydrogen-bonded SMM building blocks,[54] in our own work we have reported systems with enhanced SMM properties in cases with ferromagnetic or antiferromagnetic interactions mediated by H-bonding for Fe^{III}_6 and Fe^{III}_{19} clusters,[55] with antiferromagnetic interactions mediated by coordination bonds for Fe^{II}_6 and Fe^{III}_{13} clusters[56] and where intermolecular interactions are essentially abolished for intramolecularly ferromagnetically coupled $Mn^{II}_2Mn^{III}_2$ clusters.[57] In the particular case studied here, however, it seems that the inherent disorder of the protons involved in the hydrogen bonding plays a key role in determining the molecular rather than supramolecular properties for the SMMs.

Overall, we can conclude that the large values obtained for α in **1** probably result from strong disorder effects, in turn resulting in a broad distribution of relaxation times. Support for this is provided by the fact that similar values of α have also been obtained for the diluted complex (Table S1), ruling out the possibility of any strong effect of intermolecular interactions on the obtained value. Indeed, if the α value were the result of intermolecular interactions, then a dilution of 20% should have reduced the α value significantly as a result of diminished intermolecular interaction. Additional evidence for this conclusion comes from the estimation of the Mydosh parameter (F) in **1**, which turns out to be 0.16 for the diluted and 0.64 for the undiluted compound. The obtained large values of F rule out the spin-glass scenario of blocking of magnetization (based on intermolecular interactions), thus proving its intramolecular origin in both diluted and undiluted samples.[58] Finally, one should mention that the uncertainties in the positions of hydrogen ions in **1** may give rise to uncertainties in the direction of anisotropy axis on Dy. While we cannot estimate how much it can deviate from the calculated value in Figure 1a, we can assess changes in the dipolar interaction energy caused by such deviations. Figure S22 shows the variation of E_{dip} calculated for a large spherical sample of **1** as a function of the direction of the anisotropy axes on Dy sites. We can see that these variations take place within ± 0.16 cm^{-1}, which will not change the estimation of the order of magnitude of intermolecular interactions.

Why Is 2 Not an SMM? Having established the molecular nature of the observed dynamic magnetic behavior for **1** and **2**, the question now arises as to why the SMM behavior observed for **1** is not enhanced through the addition of the two Mn(II) S = 5/2 spins in compound **2** but, on the contrary, is quenched. The insight from the *ab initio* calculations allows us to explain the counterintuitive result that **1** is an SMM while **2** is not. Due to a very weak Dy−Mn exchange (or, generally, magnetic) interaction, the manganese ions in **2** will already have independently reorienting magnetic moments at $T = 2$ K. In this "paramagnetic regime," the latter are merely sources of a random magnetic field for the dysprosium ion, inducing the dynamics of its magnetic moment due to a tunneling splitting $\Delta_{tun} = 1/2\ \mu_B g_\perp H_\perp$. This is expected to be large, given the non-negligible values of g_X and g_Y for Dy in **2** (Table 1), as compared to **1** (Table 1) and other dysprosium complexes,[10,15,41,50] and the relatively large $H_\perp$ as compared to its typical values from intermolecular interactions.[40,59] On the contrary, $H_\perp$ is much weaker in **1**,[60] since it derives from dipolar intermolecular interactions only, while $g_\perp$ is smaller than in **2** (Table 1). In addition, the indirect contribution to the

dx.doi.org/10.1021/ic300065x | *Inorg. Chem.* 2012, 51, 9589−9597

tunneling, involving the excited states on the Dy ions (via the Zeeman interaction with the transversal field $H_{\perp}$) will also be stronger for **2** because of smaller excitation gaps on Dy in this complex (see Table S3). Since the tunneling rate of the magnetic moment is proportional to Δ_{tun}^2,[61,62] the above estimates suggest that it will be orders of magnitude larger in **2** than in **1**, explaining why the former is not an SMM. We would like to emphasize that the exchange/magnetic interaction between the metal sites becomes a source of a random transversal field for each other only in the "paramagnetic regime", when the reorientation of the local magnetic moments on each metal site becomes uncorrelated with (i.e., independent of) the reorientations of the magnetic moments on the other sites. A counterexample is the Dy_4Cr_4 compound we recently reported,[63] where the Dy(III) ions are not in the "paramagnetic regime" due to relatively strong Dy−Cr exchange interactions and which therefore shows SMM behavior despite the very large $g_{\perp}$ components in the ground Kramers doublets at the Dy sites.

CONCLUSIONS

In conclusion, by using the multidentate proligand, $\mathbf{H_4L}$, the mononuclear Dy complex **1** could be obtained. Under ESI MS conditions, the cation of compound **1** ($[Dy(H_3L)_2]^+$) showed an exchange of all 10 protic hydrogens as could be expected from its molecular structure. The reaction of compound **1** with $Mn(ClO_4)_2{\cdot}6H_2O$ in the presence of a base led to the trinuclear Mn_2Dy compound **2**. In the gas phase, doubly protonated compound **2** ($[Dy\{Mn(HL)\}_2]^+$) should display up to six H/D exchange sites, four due to the amine groups and two extra protons attached during the ESI process. However, the exchange of only two hydrogen atoms in $[Dy\{Mn(HL)\}_2]^+$ proves that these extra protons cannot be located at the free amine groups. The arrangement of the ligand structures due to incorporation of two manganese ions in changing from compound **1** to **2** obviously inhibits the HD exchange reaction with these two amines. Compound **1**, which contains a single Dy(III) ion, was found to show SMM behavior, whereas compound **2**, which incorporates a Dy(III) and two further Mn(II) ions, is a weak ferromagnet showing no SMM behavior. This result is at first sight counterintuitive, since the success of using 3d/4f blends in the search for new SMMs is usually the result of the enhanced spins provided by the 3d ions. However, the added exchange coupling in **2**, being significantly lower than the temperatures at which magnetic blocking was investigated, acts on the dysprosium ion as a fluctuating magnetic field, which causes the reversal of Dy magnetization. Put in other words, this indicates that the perceived benefit of mixing highly anisotropic Ln ions such as Dy(III) with high spin (and isotropic) 3d metal ions such as Mn(II) can be counteractive when the coupling between the 4f and 3d ions is too weak, since this can lead to the enhancement of the tunneling of magnetization on the Dy(III) ion as a result of the nature of the associated paramagnetic local fields contributed by the 3d ions. In summary, the emerging conclusion from this study is that the added transition metal ions in 3d/4f systems need to have relatively strong exchange couplings with the Ln ions in order to enhance the SMM properties, with this being the advantage of using the 3d/4f approach for producing better SMMs compared with pure 4f systems, where the coupling will always be weak.

ASSOCIATED CONTENT

Supporting Information

Details of the ESI-MS studies, magnetic measurements, computational studies, and X-ray crystallographic files in CIF format for the structure determinations of **1**−**2**. This material is available free of charge via the Internet at http://pubs.acs.org.

AUTHOR INFORMATION

Corresponding Author

*E-mail: Liviu.Chibotaru@chem.kuleuven.beannie.powell@kit.edu, yanhua.lan@kit.edu, roesky@kit.edu.

Notes

The authors declare no competing financial interest.

ACKNOWLEDGMENTS

This work was supported by the DFG-funded transregional collaborative research center SFB/TRR 88 "3MET" and Methusalem grant from K. U. Leuven. We thank Dr. M. Neumaier and Prof. Dr. H. Schnöckel for the measurement of some mass spectra. Jochen Kratsch is acknowledged for creating the cover image.

REFERENCES

(1) Christou, G.; Gatteschi, D.; Hendrickson, D. N.; Sessoli, R. *MRS Bull.* **2000**, *25*, 66.
(2) Bagai, R.; Christou, G. *Chem. Soc. Rev.* **2009**, *38*, 1011.
(3) Gatteschi, D.; Caneschi, A.; Pardi, L.; Sessoli, R. *Science* **1994**, *265*, 1054.
(4) Hewitt, I. J.; Tang, J.; Madhu, N. T.; Anson, C. E.; Lan, Y.; Luzon, J.; Etienne, M.; Sessoli, R.; Powell, A. K. *Angew. Chem., Int. Ed.* **2010**, *49*, 6352.
(5) Hewitt, I. J.; Lan, Y.; Anson, C. E.; Luzon, J.; Sessoli, R.; Powell, A. K. *Chem. Commun.* **2009**, 6765.
(6) Hussain, B.; Savard, D.; Burchell, T. J.; Wernsdorfer, W.; Murugesu, M. *Chem. Commun.* **2009**, 1100.
(7) Xu, G.-F.; Wang, Q.-L.; Gamez, P.; Ma, Y.; Clerac, R.; Tang, J.; Yan, S.-P.; Cheng, P.; Liao, D.-Z. *Chem. Commun.* **2010**, *46*, 1506.
(8) Guo, Y.-N.; Xu, G.-F.; Gamez, P.; Zhao, L.; Lin, S.-Y.; Deng, R.; Tang, J.; Zhang, H.-J. *J. Am. Chem. Soc.* **2010**, *132*, 8538.
(9) Gamer, M. T.; Lan, Y.; Roesky, P. W.; Powell, A. K.; Clerac, R. *Inorg. Chem.* **2008**, *47*, 6581.
(10) Lin, P. H.; Burchell, T.; Ungur, L.; Chibotaru, L.; Wernsdorfer, W.; Murugesu, M. *Angew. Chem., Int. Ed.* **2009**, *48*, 9489.
(11) Tang, J.; Hewitt, I.; Madhu, N. T.; Chastanet, G.; Wernsdorfer, W.; Anson, C. E.; Benelli, C.; Sessoli, R.; Powell, A. K. *Angew. Chem., Int. Ed.* **2006**, *45*, 1729.
(12) Zheng, Y.-Z.; Lan, Y.; Anson, C. E.; Powell, A. K. *Inorg. Chem.* **2008**, *47*, 10813.
(13) Abbas, G.; Lan, Y.; Kostakis, G. E.; Wernsdorfer, W.; Anson, C. E.; Powell, A. K. *Inorg. Chem.* **2010**, *49*, 8067.
(14) Westin, L. G.; Kritikos, M.; Caneschi, A. *Chem. Commun.* **2003**, 1012.
(15) Langley, S. K.; Ungur, L.; Chilton, N. F.; Moubaraki, B.; Chibotaru, L. F.; Murray, K. S. *Chem.—Eur. J.* **2011**, *17*, 9209.
(16) Ishikawa, N.; Sugita, M.; Ishikawa, T.; Koshihara, S.-y.; Kaizu, Y. *J. Phys. Chem. B* **2004**, *108*, 11265.
(17) Feltham, H. L. C.; Lan, Y.; Klöwer, F.; Ungur, L.; Chibotaru, L. F.; Powell, A. K.; Brooker, S. *Chem.—Eur. J.* **2011**, *17*, 4362.
(18) Luis, F.; Martínez-Pérez, M. J.; Montero, O.; Coronado, E.; Cardona-Serra, S.; Martí-Gastaldo, C.; Clemente-Juan, J. M.; Sesé, J.; Drung, D.; Schurig, T. *Phys. Rev. B* **2010**, *82*, 060403.
(19) Takamatsu, S.; Ishikawa, T.; Koshihara, S.-y.; Ishikawa, N. *Inorg. Chem.* **2007**, *46*, 7250.
(20) Ishikawa, N. *Polyhedron* **2007**, *26*, 2147.
(21) Bernot, K.; Pointillart, F.; Rosa, P.; Etienne, M.; Sessoli, R.; Gatteschi, D. *Chem. Commun.* **2010**, *46*, 6458.

(22) AlDamen, M. A.; Clemente-Juan, J. M.; Coronado, E.; Martí-Gastaldo, C.; Gaita-Ariño, A. *J. Am. Chem. Soc.* **2008**, *130*, 8874.
(23) AlDamen, M. A.; Cardona-Serra, S.; Clemente-Juan, J. M.; Coronado, E.; Gaita-Arinño, A.; Martí-Gastaldo, C.; Luis, F.; Montero, O. *Inorg. Chem.* **2009**, *48*, 3467.
(24) Ishikawa, N.; Sugita, M.; Ishikawa, T.; Koshihara, S.-y.; Kaizu, Y. *J. Am. Chem. Soc.* **2003**, *125*, 8694.
(25) Jiang, S.-D.; Wang, B.-W.; Su, G.; Wang, Z.-M.; Gao, S. *Angew. Chem., Int. Ed.* **2010**, *49*, 7448.
(26) Jiang, S.-D.; Wang, B.-W.; Sun, H.-L.; Wang, Z.-M.; Gao, S. *J. Am. Chem. Soc.* **2011**, *133*, 4730.
(27) Sessoli, R.; Powell, A. K. *Coord. Chem. Rev.* **2009**, *253*, 2328.
(28) Glaser, T. *Chem. Commun.* **2011**, *47*, 116.
(29) Pointillart, F.; Bernot, K.; Sessoli, R.; Gatteschi, D. *Chem.—Eur. J.* **2007**, *13*, 1602.
(30) Sheldrick, G. M. *Acta Crystallogr., Sect. A* **2008**, *64*, 112.
(31) Aquilante, F.; De Vico, L.; Ferré, N.; Ghigo, G.; Malmqvist, P.-Å.; Neogrády, P.; Pedersen, T. B.; Pitoňák, M.; Reiher, M.; Roos, B. O.; Serrano-Andrés, L.; Urban, M.; Veryazov, V.; Lindh, R. *J. Comput. Chem.* **2010**, *31*, 224.
(32) Avogadro, Version 1.0. http://avogadro.openmolecules.net/wiki/Main_Page (accessed Mar. 2012).
(33) Douglas, M.; Kroll, N. M. *Ann. Phys.* **1974**, *82*, 89.
(34) Hess, B. A. *Phys. Rev. A* **1986**, *33*, 3742.
(35) Malmqvist, P.-Å.; Roos, B. O.; Schimmelpfennig, B. *Chem. Phys. Lett.* **2002**, *357*, 230.
(36) Chibotaru, L. F.; Ungur, L.; Aronica, C.; Elmoll, H.; Pilet, G.; Luneau, D. *J. Am. Chem. Soc.* **2008**, *130*, 12445.
(37) Ungur, L.; Van den Heuvel, W.; Chibotaru, L. F. *New J. Chem.* **2009**, *33*, 1224.
(38) Lines, M. E. *J. Chem. Phys.* **1971**, *55*, 2977.
(39) Chibotaru, L. F.; Ungur, L. *POLY ANISO*; University of Leuven: Leuven, Belgium, 2006.
(40) Lin, P.-H.; Burchell, T. J.; Clérac, R.; Murugesu, M. *Angew. Chem., Int. Ed.* **2008**, *47*, 8848.
(41) Long, J.; Habib, F.; Lin, P.-H.; Korobkov, I.; Enright, G.; Ungur, L.; Wernsdorfer, W.; Chibotaru, L. F.; Murugesu, M. *J. Am. Chem. Soc.* **2011**, *133*, 5319.
(42) Habib, F.; Lin, P.-H.; Long, J.; Korobkov, I.; Wernsdorfer, W.; Murugesu, M. *J. Am. Chem. Soc.* **2011**, *133*, 8830.
(43) Weismann, D.; Sun, Y.; Lan, Y.; Wolmershäuser, G.; Powell, A. K.; Sitzmann, H. *Chem.—Eur. J.* **2011**, *17*, 4700.
(44) Rinehart, J. D.; Long, J. R. *J. Am. Chem. Soc.* **2009**, *131*, 12558.
(45) Rinehart, J. D.; Meihaus, K. R.; Long, J. R. *J. Am. Chem. Soc.* **2010**, *132*, 7572.
(46) Freedman, D. E.; Harman, W. H.; Harris, T. D.; Long, G. J.; Chang, C. J.; Long, J. R. *J. Am. Chem. Soc.* **2010**, *132*, 1224.
(47) Rinehart, J. D.; Long, J. R. *J. Am. Chem. Soc.* **2009**, *131*, 12558.
(48) Freedman, D. E.; Harman, W. H.; Harris, T. D.; Long, G. J.; Chang, C. J.; Long, J. R. *J. Am. Chem. Soc.* **2010**, *132*, 1224.
(49) Car, P.-E.; Perfetti, M.; Mannini, M.; Favre, A.; Caneschi, A.; Sessoli, R. *Chem. Commun.* **2011**, *47*, 3751.
(50) Guo, Y.-N.; Xu, G.-F.; Wernsdorfer, W.; Ungur, L.; Guo, Y.; Tang, J.; Zhang, H.-J.; Chibotaru, L. F.; Powell, A. K. *J. Am. Chem. Soc.* **2011**, *133*, 11948.
(51) It is interesting to note that the calculated E_{dip} is on the same order of magnitude as the interaction between two nearest neighbor Dy ions (see Figure S20 and Table S8). It is evident, therefore, that the calculated values of E_{dip} in Figure 4 and of zJ are the result of strong compensation between the contributions of individual pairs. This is not surprising if we remember that, for lattices of cubic symmetry, E_{dip} should be exactly zero,[52] for any orientations of (parallel) anisotropy axes on the magnetic ions.
(52) Ashcroft, N. W.; Mermin, D. N. *Solid State Physics*; Saunders College: Philadelphia, 1988.
(53) Petit, S.; Pilet, G.; Luneau, D.; Chibotaru, L. F.; Ungur, L. *Dalton Trans.* **2007**, *40*, 4582.
(54) (a) Wernsdorfer, W.; Aliaga-Alcalde, N.; Hendrickson, D. N.; Christou, G. *Nature* **2002**, *416*, 406. (b) Tiron, R.; Wernsdorfer, W.; Foguet-Albiol, D.; Aliaga-Alcalde, N.; Christou, G. *Phys. Rev. Lett.* **2003**, *91*, 227203. (c) Hill, S.; Edwards, R. S.; Aliaga-Alcalde, N.; Christou, G. *Science* **2003**, *302*, 1015.
(55) Affronte, M.; Sessoli, R.; Gatteschi, D.; Wernsdorfer, W.; Lasjaunias, J. C.; Heath, S. L.; Powell, A. K.; Fort, A.; Rettori, A. *J. Phys. Chem. Solids* **2004**, *65*, 745.
(56) (a) Fei, B.-L.; Clérac, R.; Anson, C. E.; Powell, A. K. *Dalton Trans.* **2005**, 1381. (b) Murugesu, M.; Clérac, R.; Wernsdorfer, W.; Anson, C. E.; Powell, A. K. *Angew. Chem., Int. Ed.* **2005**, *44*, 6678.
(57) Ako, A. M.; Mereacre, V.; Hewitt, I. J.; Clérac, R.; Lecren, L.; Anson, C. E.; Powell, A. K. *J. Mater. Chem.* **2006**, *16*, 2579.
(58) Gatteschi, D.; Sessoli, R.; Villain, J. *Molecular Nanomagnets*; Oxford University Press: Oxford, U. K., 2006.
(59) Besides the dipolar magnetic contributions from $S = 5/2$ of Mn1 and Mn2, there is also a contribution of the superexchange Mn1−Dy and Mn2−Dy interaction to Δ_{tun}.
(60) Generally, the value of the transversal field $H_{\perp}$ at the location point of the Dy ion in **1** and **2** scales with the strength of its magnetic interaction with the surrounding magnetic ions. The latter is proportional to the exchange splitting arising from the interaction of Dy ion (effective $S = 1/2$) with surrounding metal ions, which is 1.2 cm^{-1} in **2** (see the bottom of Table S7) and $2E_{pol} = 0.12$ cm^{-1} in **1** (see Figure 4a). Thus, the transversal field is expected to be 1 order of magnitude stronger in **2** than in **1**.
(61) Prokof'ev, N. V.; Stamp, P. C. E. *Phys. Rev. Lett.* **1998**, *80*, 5794.
(62) Prokof'ev, N. V.; Stamp, P. C. E. *Rep. Prog. Phys.* **2000**, *63*, 669.
(63) Rinck, J.; Novitchi, G.; Van den Heuvel, W.; Ungur, L.; Lan, Y.; Wernsdorfer, W.; Anson, C. E.; Chibotaru, L. F.; Powell, A. K. *Angew. Chem., Int. Ed.* **2010**, *49*, 7583.